Available online at www.sciencedirect.com
SCIENCE DIRECT®
Chaos, Solitons and Fractals 20 (2004) 863–876
CHAOS SOLITONS & FRACTALS
www.elsevier.com/locate/chaos

Towards reaction–diffusion computing devices based on minority-carrier transport in semiconductors

Tetsuya Asai [a,*], Andrew Adamatzky [b], Yoshihito Amemiya [a]

[a] Department of Electrical Engineering, Hokkaido University, Kita 13, Nishi 8, Kita-ku, Sapporo 060-8628, Japan
[b] Faculty of Computing, Engineering and Mathematical Sciences, University of the West of England, Bristol BS16 1QY, UK

Accepted 10 October 2003

Abstract

Reaction–diffusion (RD) chemical systems are known to realize sensible computation when both data and results of the computation are encoded in concentration profiles of chemical species; the computation is implemented via spreading and interaction of either diffusive or phase waves. Thin-layer chemical systems are thought of therefore as massively-parallel locally-connected computing devices, where micro-volume of the medium is analogous to an elementary processor. Practical applications of the RD chemical systems are reduced however due to very low speed of traveling waves which makes real-time computation senseless. To overcome the speed-limitations while preserving unique features of RD computers we propose a semiconductor RD computing device where minority carriers diffuse as chemical species and reaction elements are represented by p–n–p–n diodes. We offer blue-prints of the RD semiconductor devices, and study in computer simulation propagation phenomena of the density wave of minority carriers. We then demonstrate what computational problems can be solved in RD semiconductor devices and evaluate space–time complexity of computation in the devices.

1. Introduction

Despite dramatic technological progress of digital processors and semiconductor integrated circuits, fundamental principles of their computing operations remain unchanged for the decades: the computational devices have ''rigid'' physical architectures vulnerable to almost any kind of damage and the perform calculation in a systematic fashion under precise timing control. Natural systems give us examples of amorphous, unstructured, devices capable for fault-tolerant information processing particularly with regard to massive parallel spatial problems that digital processors are rather weak in.

Reaction–diffusion (RD) chemical systems are well known now for their unique ability to efficiently solve combinatorial problems with natural parallelism [2]. In liquid-phase parallel processors, both the data and the results of the computation are encoded as concentration profiles of the reagents, the computation per se is performed via the spreading and interaction of wave fronts. In experimental chemical processors data are represented by local disturbances of concentrations and computation is implemented via the interaction of waves caused by the local disturbances. The RD chemical computers are parallel because the chemical medium's micro-volumes update their states simultaneously, and molecules diffuse and react in parallel.

* Corresponding author. Tel.: +81-11-706-6080; fax: +81-11-706-7890.
E-mail address: asai@sapiens-ei.eng.hokudai.ac.jp (T. Asai).
URL: http://www.sapiens-ei.eng.hokudai.ac.jp.

0960-0779/$ - see front matter © 2003 Elsevier Ltd. All rights reserved.
doi:10.1016/j.chaos.2003.09.041

RD information processing in chemical media became a hot subject of not simply theoretical but also experimental investigations after Kuhnert et al. [27] implemented basic operations of image processing in light-sensitive Belousov–Zhabotinsky (BZ) reaction. During the last decade experimental prototypes of RD computing devices were fabricated and applied to solve various problems of computer science, including image processing [4,27,36,38], pattern recognition [4,16,24–26,47], path planning [8,10,37,39] and robot navigation [6] and many more (see overview in [2]). Computational universality of RD chemical media was demonstrated in series of works in implementation of logical gates and diodes in excitable (BZ system) [14,22–24,26,29–31,39,43] and non-excitable [7] chemical media; and, possible implementation of memory units in BZ medium is discussed in [30].

Practical value of RD chemical systems are significantly reduced by low speed of traveling waves which makes real-time computation senseless. One of the cost-efficient options to overcome the speed-limitations of RD computers while preserving unique features of wave-based computing is to implement RD chemical computers in silicon. The velocity of traveling wavefronts in typical reaction diffusion systems, e.g., BZ reaction, is 10^{-2} m/s [42], while that of a hardware RD system will be over a million times faster than that of the BZ reaction, independent of system size [11,12]. The increase in speed will be indispensable for developers of RD computers. Moreover, if a RD system is implemented in integrated circuits, then we would be able to artificially design various types RD spatio-temporal dynamics (the types may never occur in real-life chemical systems) and thus develop parallel computing processors for novel applications. Basing on experimental evidences of RD-like behaviour, namely traveling current density filaments [33,34], in p–n–p–n devices we propose a novel type of semiconductor RD computing device, where minority carriers diffuse as chemical species and reaction elements are represented by p–n–p–n diodes.

2. A reaction–diffusion device using minority-carrier transport

In forwardly biased p–n junctions, minority carriers are generated in both area of p- and n-type semiconductors, as shown in Fig. 1. For p-type semiconductors, the minority carriers are electrons, while they are holes in n-type semiconductors. Once minority carriers are generated, they diffuse among the semiconductor and finally disappears by the recombination of electrons and holes as

$$\frac{\partial n(\mathbf{r},t)}{\partial t} = D_n \nabla^2 n(\mathbf{r},t) - \frac{n(\mathbf{r},t)}{\tau}, \tag{1}$$

where n represents the density of minority carriers, $\mathbf{r}$ the space, t the time, $D_n \equiv \mu kT/q$ (μ is the mobility of carriers, k the Boltzmann's constant, T the temperature, q the electron charge), and τ the lifetime of the minority carriers [40]. We now regard the minority carriers as one chemical substance, i.e., electrons in the p-type semiconductor because Eq. (1) has the same form as the reaction–diffusion equation [32].

To construct an active RD device, we implement a number of "sources" of minority carriers regularly arranged on a common semiconductor die (substrate), as shown in Fig. 2. We call the source a *reaction device*. Minority carriers produced at a reaction device will travel through the substrate by diffusion and reach the adjacent reaction devices. To generate minority carriers on diffusive medium, we employ a p–n–p–n device, which is a traditional semiconductor device used as triac, thyristors and so on [40], in each reaction device. We briefly review operations of the device in the following subsections.

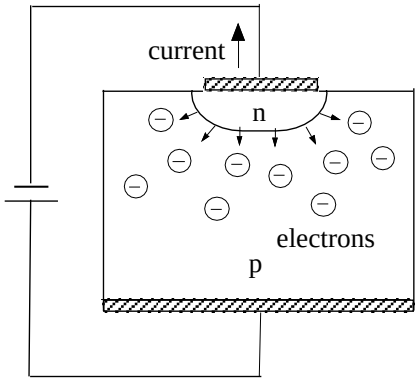

Fig. 1. Minority-carrier diffusion in forwardly-biased p–n junction.

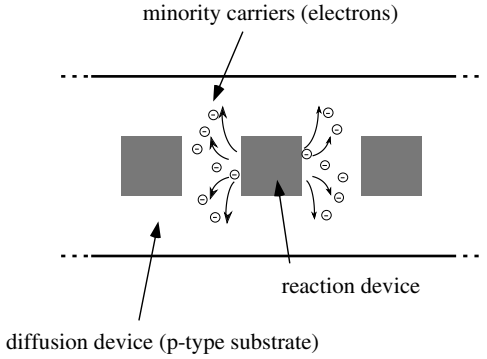

Fig. 2. Construction of RD device that consists of a number of "sources" of minority carriers regularly arranged on a common semiconductor die.

2.1. A brief review of p–n–p–n device operation

Let us consider bias condition of a p–n–p–n device shown in Fig. 3. In this condition, p^+–n and p–n^+ junctions are forwardly biased, while n–p junction is reversely biased. So, the flow of majority carriers, which generate current flow i, are blocked at this n–p junction. The device is thus off state and electrons as minority carriers are generated in the p region. They diffuse this region and disappear within a given time constant by the recombination with holes.

Assume that a seed electron is given to the p region and it diffuses among the region ((a) in Fig. 3). If the electron is not disappeared by recombination accidentally and it induces several holes from p^+ region ((b) in Fig. 3), each hole also induces multiple electrons from n^+ region ((c) in Fig. 3). This results in the autocatalytic multiplication of electrons in the p region. If the p region is fulfilled with electrons, the p region is inverted to n-type semiconductor. This causes the transition of the p–n–p–n device from off to on state because the reversely-biased n–p junction become just a n–n junction at this state. The initial density of electrons in the region determines a threshold voltage at which the device is turned on. The voltage is called a breakover voltage. Fig. 4 shows typical current-voltage characteristics of a p–n–p–n device. If voltage V exceeds the breakover voltage (V_B), the device is suddenly turned on.

Once the p–n–p–n device is turned on, it can not be turned off until the supply voltage V is cut off. When V is set to zero, electrons in the p region (now it is inverted to n type) disappears due to the recombination. As a result, the device returns to the resting (off) state.

2.2. A heuristic model of p–n–p–n device

We here propose a simple model of p–n–p–n device for large-scale numerical simulation because the RD device we propose consists of large number of reaction devices.

Let us assume that the p–n–p–n device is a non-linear resistive device. Its resistance is defined by

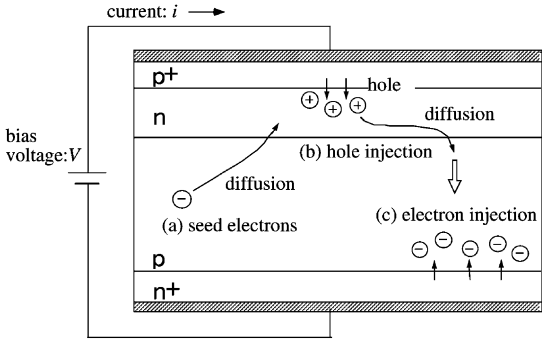

Fig. 3. Autocatalytic multiplication of minority carriers (electrons) in the p–n–p–n device.

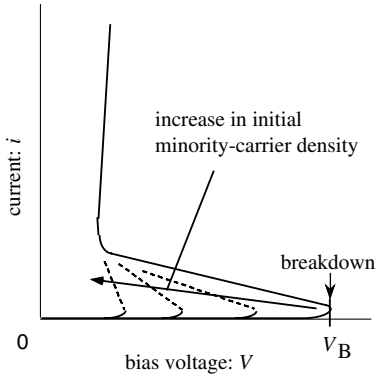

Fig. 4. Voltage–current characteristic of typical p–n–p–n device.

$$R(V,n)=\begin{cases} R_{\text{off}} & (\text{if } V < V_B(n)),\\ R_{\text{on}} + (R_{\text{off}} - R_{\text{on}}) \exp\left(-\frac{V - V_B(n)}{V_0}\right) & (\text{else}), \end{cases} \tag{2}$$

where V represents the bias voltage, n the density of minority carriers (electrons) in the p region of a p–n–p–n device, R_{off} (or R_{on}) the resistance of the device in off (or on) state and $V_B(n)$ the breakover voltage as a function of n. If $V < V_B(n)$, the device is turned off with high resistance (R_{off}), while the device is turned on $[R(V,n) \to R_{\text{on}}]$ when $V > V_B(n)$, as shown in Fig. 5(a). Its on-off sensitivity is determined by constant voltage V_0. This imitates the characteristics of the sudden change of resistance (V/i) in Fig. 4.

As described in previous subsection, the breakover voltage is a function of n. We define the function as

$$V_B(n)=\begin{cases} V_B^{\max} & (\text{if } n < n_{\text{th}}),\\ V_B^{\min} + (V_B^{\max} - V_B^{\min}) \exp\left(-\frac{n - n_{\text{th}}}{n_0}\right) & (\text{else}), \end{cases} \tag{3}$$

where $V_B^{\max}$ (or $V_B^{\min}$) represents the maximum (or minimum) breakover voltage, n_{th} the threshold density and n_0 the sensitivity of the change of the breakover voltage. When $n < n_{\text{th}}$, the breakover voltage does not change ($V_B = V_B^{\max}$), while the voltage decrease to $V_B^{\min}$ exponentially when $n > n_{\text{th}}$ (Fig. 5(b)). This imitates the change of the breakover voltage with the value of n in Fig. 4.

2.3. The RD device using p–n–p–n devices

The reaction device we propose is illustrated in Figs. 6 and 7. The device structure shown in Fig. 6 is designed for one-dimensional RD device that can be fabricated with conventional CMOS technology. Fig. 6(a) and (b) show the top view and cross-sectional view of the device along with a dashed line A in Fig. 6(a). A p–n–p–n device is laterally

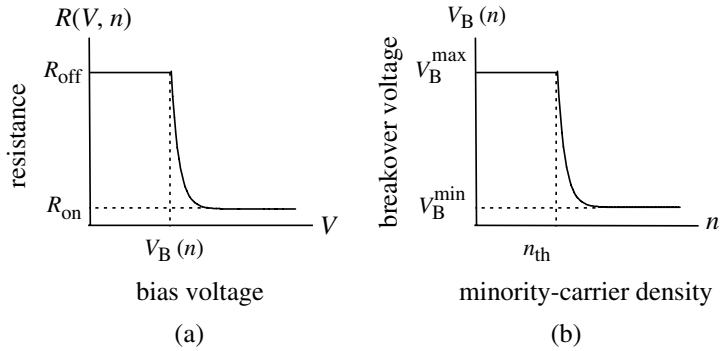

Fig. 5. Threshold functions of p–n–p–n device model; (a) non-linear resistance against breakover voltage and (b) the breakover voltage against minority-carrier density.

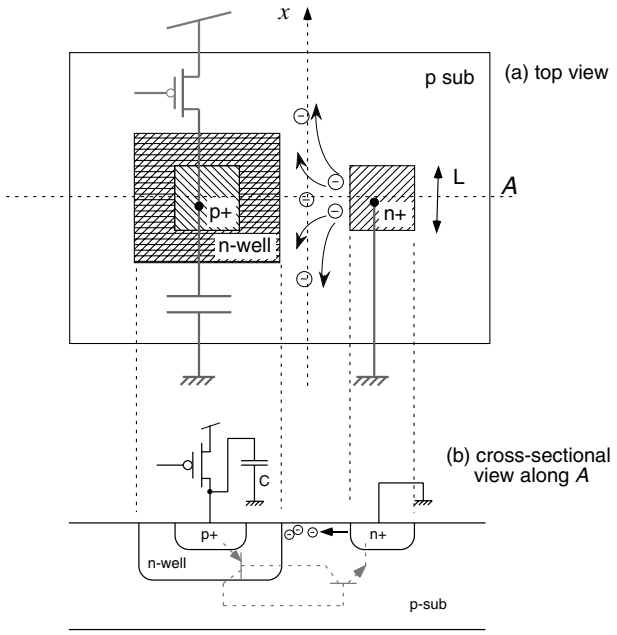

Fig. 6. Construction of one-dimensional RD device suitable for conventional CMOS technology.

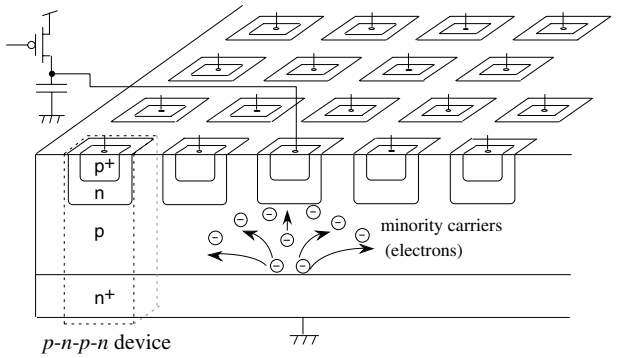

Fig. 7. Construction of two-dimensional RD device with vertical p–n–p–n devices.

constructed beneath the substrate surface. On the other hand, the device structure shown in Fig. 7 is designed for two-dimensional RD device. A p–n–p–n device is constructed vertically. It will require some special processes for actual fabrication. In both constructions above, minority carriers (electrons) produced at a p region in a p–n–p–n device will travel through the p-type common area by diffusion.

The p–n–p–n device is connected with a capacitor and a pMOS FET acting as a current source. Fig. 8 shows its equivalent circuit. This combination of a p–n–p–n device, a capacitor and a pMOS FET is the unit construction of the proposed RD device. We call this unit a *reaction cell*.

The dynamics of a reaction cell is given by

$$C\frac{\mathrm{d}v}{\mathrm{d}t} = I_{\mathrm{b}}(v) - \frac{v}{R(v,n)}, \tag{4}$$

$$q\frac{\mathrm{d}n}{\mathrm{d}t} = -q\frac{n}{\tau} + \frac{v}{R(v,n)}, \tag{5}$$

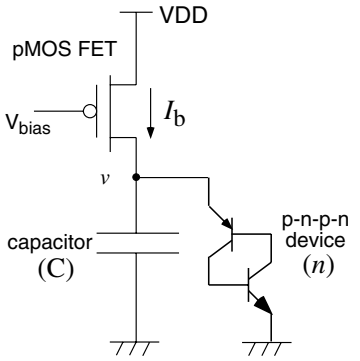

Fig. 8. Equivalent circuit of a reaction cell.

where C represents the capacitance, v the capacitor voltage, n the minority carrier density, q the charge of electron, R the resistance of the p–n–p–n device defined by Eq. (2), $I_b(v)$ the current of pMOS FET as a function of v and τ the minority carrier lifetime. The current of pMOS FET is given by

$$I_b(v) = I_0 \exp\left(\kappa \frac{\mathrm{VDD} - V_{bias}}{V_T}\right)\left(1 - \exp\left(-\frac{\mathrm{VDD} - v}{V_T}\right) + \frac{\mathrm{VDD} - v}{V_0}\right), \tag{6}$$

where VDD represents the supply voltage, V_{bias} the gate voltage of the pMOS FET, I_0 the MOS fabrication parameter, κ the effectiveness of the gate potential, $V_T \equiv kT/q \approx 26$ mV at room temperature [44]. In Eqs. (4) and (5), we assume that capacitor charge decreases by the amount equal to the increased minority carriers. It should be noted that this device imitates a substrate-depleted reaction because the charge of the capacitor is depleted by the p–n–p–n device.

The reaction cell can be oscillatory (astable) or excitatory (monostable) depending on supply voltage VDD. It is oscillatory if VDD is higher than breakover voltage V_B of the p–n–p–n device, and excitatory if VDD is lower than V_B. In the oscillatory condition (VDD $> V_B$), the capacitor is charged by bias current $I_b(v)$ and consequently, capacitor charge increases until capacitor voltage v reaches breakover voltage V_B. When v reaches V_B, the breakover of the p–n–p–n device starts and minority carriers are injected from the n^+ region to the p region. Then, the autocatalytic multiplication of minority carriers occurs to turn the device on. The stored charge on the capacitor flows into the device, so capacitor charge (therefore capacitor voltage v) decreases and consequently, the device is turned off. The reaction cell repeats this cycle and produces oscillatory dynamics. On the other hand, in the excitatory condition (VDD $< V_B$), capacitor voltage v cannot reach breakover voltage V_B because v does not exceed supply voltage VDD (bias current $I_b(v)$ becomes 0 when v increases up to VDD). In this condition, the p–n–p–n device turns on only when minority carriers are injected from outside; i.e., neighboring cells.

Fig. 9 shows one-dimensional RD device with multiple reaction devices on a common substrate. Each reaction devices are labeled as Rn (n is the index number), while diffusion areas are labeled as D. Minority-carriers (electrons) produced by each reaction device will travel through the diffusion area (p-sub region) by diffusion and reach adjacent devices. When the reaction devices are closely arranged on the substrate, these minority carriers will induce a chain reaction among the reaction devices. We can estimate the minimum distance between adjacent devices to cause the chain reaction as the following.

The dynamics of minority-carriers along with the x-axis in Fig. 9 are governed by Eq. (1). The impulse response to Eq. (1) is

$$g(x) = \frac{1}{\sqrt{4\pi D_n t}} \exp\left(-\frac{x^2}{4D_n t} - \frac{t}{\tau}\right). \tag{7}$$

When reaction device R1 turns on at $t = 0$, the minority-carrier concentrates around the reaction device ($n(x,0)$ in Fig. 10). The total amount of the minority carriers in the p–n–p–n device is assumed to be equal to the charge of the capacitor at $t = 0$. The minority carrier distribution $n(x,t)$ is thus obtained as

$$n(x,t) = n(x,0) * g(x) = \frac{N_0}{2} \exp\left(-\frac{t}{\tau}\right)\left[\mathrm{erf}\left(\frac{x + L/2}{\sqrt{4D_n t}}\right) - \mathrm{erf}\left(\frac{x - L/2}{\sqrt{4D_n t}}\right)\right], \tag{8}$$

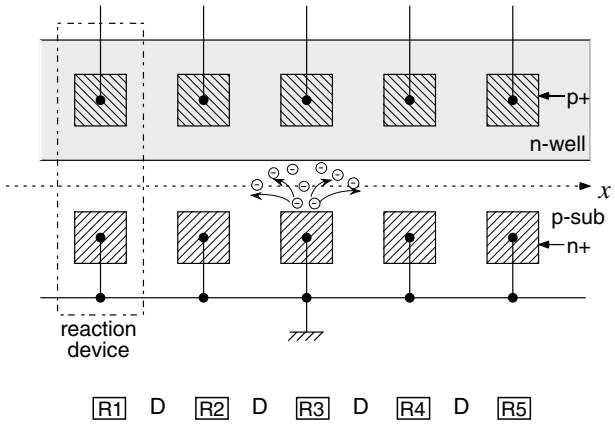

Fig. 9. Experimental settings for one-dimensional RD device.

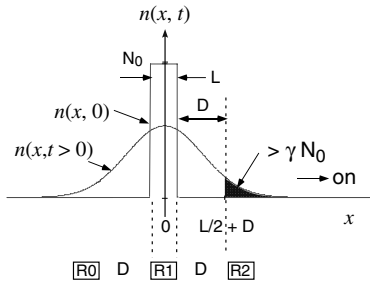

Fig. 10. Diffusion of minority carriers around an active cell (R1).

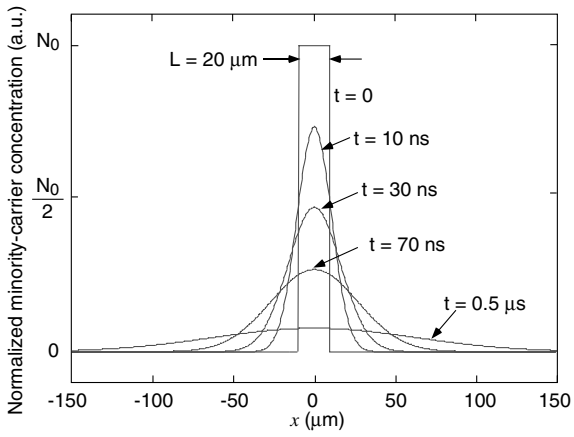

Fig. 11. Diffusion of minority carriers within typical semiconductor (silicon) device.

where L and N_0 represent the length of the reaction device (See Fig. 6(a)) and the total amount of the charge of the capacitor ($= C\mathrm{VDD}/q$), respectively.

Let us assume that the reaction device turns on when the total amount of the minority carriers in the p–n–p–n device exceeds the amount of γN_0. As shown in Fig. 10, minority carriers produced by reaction device R1 will turn on its adjacent device R2 when

$$\int_{D+L/2}^{\infty} n(x,t) \geqslant \gamma N_0, \tag{9}$$

where D is the distance between adjacent reaction devices. With a given γ, one can briefly estimate the RD device geometries (L and D). Fig. 11 shows example plots of Eq. (8) with practical device parameters ($D_n = 39$ cm^2/s ($\mu_n = 1500$ cm^2/V s), $\tau = 1$ μs and $L = 20$ μm).

3. Simulation results

For simplification of numerical simulation, we normalize the capacitor voltage and minority-carrier density in Eqs. (4) and (5). The resultant equations are

$$\frac{\mathrm{d}u}{\mathrm{d}t} = k_0 i(u) - \frac{u}{r(u,v)}, \tag{10}$$

$$\frac{\mathrm{d}v}{\mathrm{d}t} = -v + \frac{u}{r(u,v)}, \tag{11}$$

where

$$i(u) = 1 - \exp(k_1(u-1)) + k_2(1-u), \tag{12}$$

$$r(u,v) = \begin{cases} r_{\mathrm{off}} & (\text{if } u < v(n)), \\ r_{\mathrm{on}} + (r_{\mathrm{off}} - r_{\mathrm{on}}) \exp\left(-\frac{u-v(n)}{\alpha}\right) & (\text{else}), \end{cases} \tag{13}$$

$$v(n) = \begin{cases} x_b & (\text{if } v < x_s), \\ x_f + (x_b - x_f) \exp\left(-\frac{v-x_s}{\beta}\right) & (\text{else}). \end{cases} \tag{14}$$

In the following simulations, we use parameter values obtained from typical p–n–p–n device. The normalized values are: $r_{\mathrm{on}} = 10^{-2}$, $r_{\mathrm{off}} = 10^4$, $\alpha = \beta = 40$, $x_b = 0.8$ (for oscillatory mode) ~1.2 (for excitatory mode), $x_f = 0.2$, $x_s = 0.02$, $r_{\mathrm{on}} = 10^{-2}$, $r_{\mathrm{on}} = 10^{-2}$, $k_0 = 0.05$, $k_1 = 25$ and $k_2 = 0.2$.

Fig. 12 illustrate numerical solutions to Eqs. (10) and (11). Fig. 12(a) shows the relaxation oscillations of a reaction cell in variables u and v. Fig. 12(b) shows the excitatory behaviour of the reaction cell. The cell settles down in the stable state of $u = 1$ and $v = 0$, and no further change occurs as long as minority carriers are not injected. In the simulation, minority carriers were injected from the outside at $t = 50$. Triggered by this injection, the p–n–p–n device turned on for once, and then returned to the stable state.

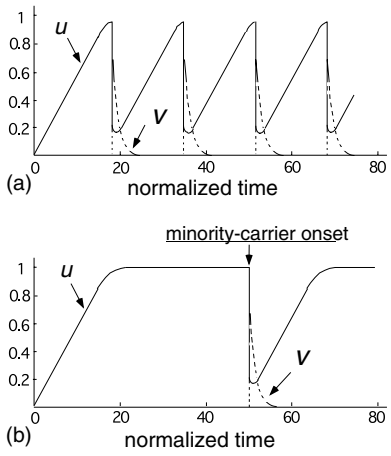

Fig. 12. Simulation results of reaction cell for (a) oscillatory mode and (b) excitatory mode.

We confirmed the operation of the one-dimensional RD device. The RD equation was obtained along with the x-axis in Fig. 6. At the position of each reaction device, we solve the following RD equations:

$$\frac{\partial u}{\partial t} = k_0 i(u) - \frac{u}{r(u,v)}, \tag{15}$$

$$\frac{\partial v}{\partial t} = D_n \frac{\partial^2 v}{\partial x^2} - v + \frac{u}{r(u,v)}. \tag{16}$$

In other positions where no reaction device exists, we solve the following equations:

$$\frac{\partial u}{\partial t} = 0, \quad \frac{\partial v}{\partial t} = D_n \frac{\partial^2 v}{\partial x^2} - v. \tag{17}$$

We solve the equations above by using three-point approximation of the Laplacian on the one-dimensional grid and the fourth-order Runge–Kutta method. At each side of the reaction-space, we applied the Neumann boundary condition:

$$\nabla[u] = \nabla[v] = (0,0), \tag{18}$$

where $\nabla = (\partial/\partial x)$.

Fig. 13 shows a result for the one-dimensional RD device with nine reaction devices. In the simulations, we assume $x_b = 1.2$ (excitatory mode), $\gamma = 0.1$ and $D_n = 20 \times 10^{-6}$. In Fig. 13, horizontal and vertical axes represent the normalized space and the time, respectively. The position of the reaction device is indicated by Rn ($n = 1, 2, \ldots, 9$) at the bottom.

At an initial state ($t = 0$), a center reaction device produced minority carriers. The carriers are diffused around the reaction device, and at $t \approx 25$, its adjacent devices are turned on (activated). They produce minority carriers as well, then at $t \approx 50$ (80), their adjacent reaction devices are activated. The propagating waves are produced in the form of the propagation of the activations of reaction devices.

Very slow decay of the minority carrier concentration was observed in a reaction device being activated by its adjacent device. Fig. 14 shows time course of the concentration of the reaction device. The normalized refractory period was the order of 1. It was approximately hundred times as long as the propagating time between the adjacent reaction devices. Note that the decay time can be controlled by ejecting minority carriers from the p-sub region.

Next, we designed two-dimensional RD device by arranging the reaction cells on a plane and specifying the device operation. The same set of reaction–diffusion equations as Eqs. (15)–(17), where the diffusion terms were expanded to two-dimension (x, y), were solved by five-point approximation of the Laplacian on the two-dimensional grid and the fourth-order Runge–Kutta method. At each side of the reaction-space, we applied the Neumann boundary condition. Fig. 15 shows a result for a device with 200×200 excitatory reaction cells. The spatial density of minority carriers is represented in gray scale ($v = 0$: black, $v = 1$: white). With periodic injection of minority carriers at a point (P in

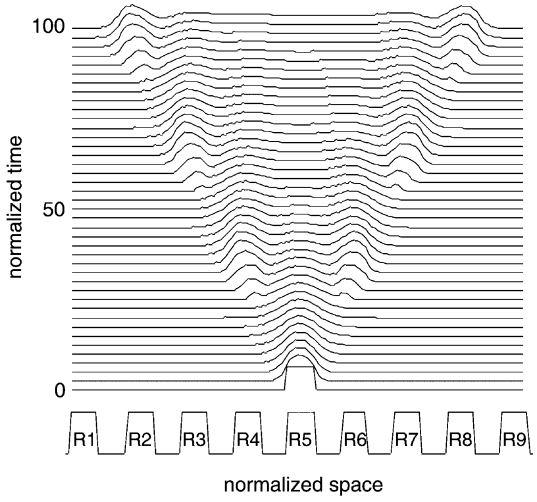

Fig. 13. Active wave propagation on one-dimensional RD device.

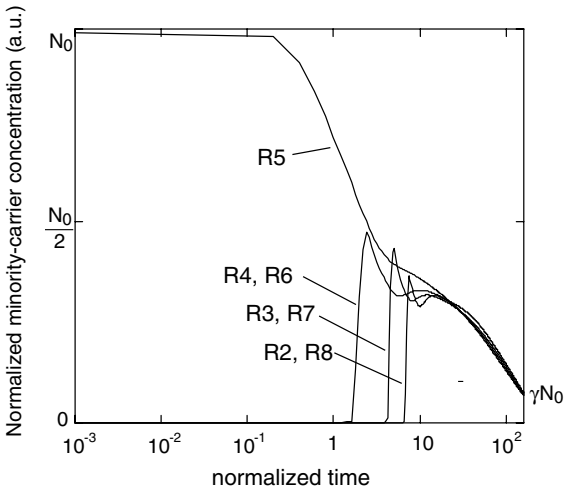

Fig. 14. Temporal changes of concentration of minority carriers during the wave propagation.

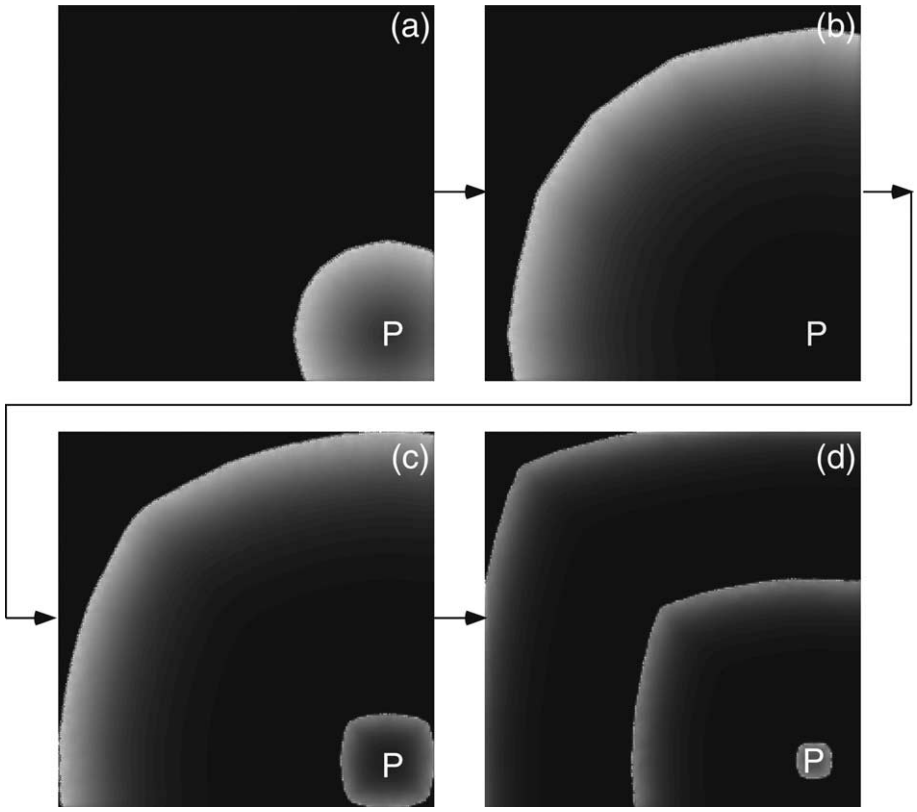

Fig. 15. Simulation results of the two-dimensional RD device producing target patterns.

Fig. 15), the RD device produced spreading concentric waves of minority carriers. This results indicate that the injected carriers diffused around the injection point and successfully induced a chain of reactions of the cells.

Fig. 16 shows a result of the excitatory RD device without external injections of minority carriers. With an appropriate initial pattern of minority-carrier densities, the RD device produced rotating spiral patterns of minority

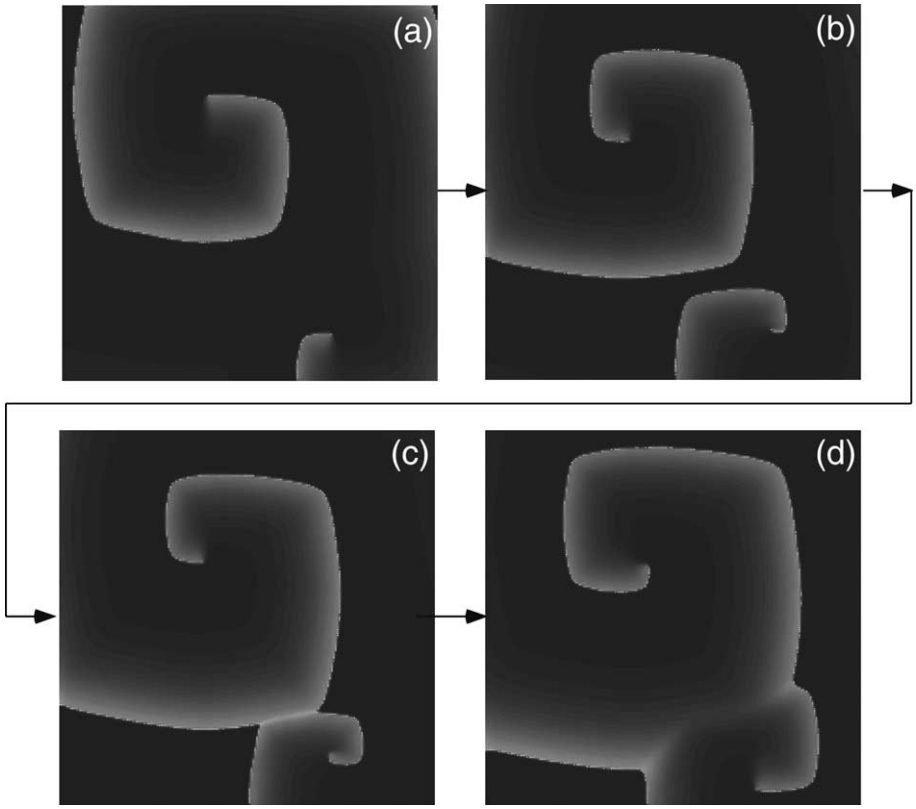

Fig. 16. Simulation results of the two-dimensional RD device producing spiral waves.

carriers. Notice that the wave disappears at collision points (Fig. 16(c)–(d)) because of the depletion of minority carriers. This is the same phenomenon as observed in natural RD systems.

4. Computing in RD semiconductor devices

Now we understand how the RD semiconductor device behaves however we still need to specify how its computation operational characteristics. A RD computation, particularly in active chemical media, is implemented by traveling waves which interact with, or collide to, each other and form a dynamical, e.g. oscillating pattern, or stationary, e.g. precipitate concentration profile, structure. This structure represents result of the computation, while data are represented by initial configuration of wave generators.

Before starting any computation one should input data-information in the RD medium. A parallel input is an essential feature of an edge-cutting parallel computing architecture. Serial inputs, so common for vast majority of massively-parallel processors], dramatically decrease performance of the computing devices, particularly those operating in transducer mode, where information is constantly fed into the processor (e.g. in tasks of image processing). Experimental RD chemical computers, at least in certain case, may well have analogs of parallel inputs. It has been demonstrated widely that applying light of varying intensity we can control excitation dynamic in BZ-medium [13,19,21,35], wave velocity [41], patter formation [45]. Of particular interest are experimental evidences of light-induced back propagating waves, wave-front splitting and phase shifting [46]; we can also manipulate medium's excitability by varying intensity of the medium's illumination [15]. In fact, optical input of data-information has been already used at the beginning of RD research [27]. This was proved to particularly important in experiments in image processing in BZ-medium-based computing devices [27,36–38]. We are not aware of any rigorous experimental results demonstrating a possibility of optical inputs of RD semiconductor devices there is however a simulation-related evidence of a possibility of optical parallel inputs. Paper [28] discusses particulars of a photo-response, photon-induced generation of electron-hole

pairs in p–n–p–n devices, depending on primary colour components in the stimulating input because elementary processors can also act as colour sensors.

There exists a possibility of parallel optical outputs on semiconductor devices. Technologies for integrating optoelectronic devices and electronic circuitry are fully developed, but limited hybrid integration is available commercially at present. An important problem of such integration is that pursuing it involves simultaneous development of sophisticated technologies for optoelectronic devices (III–V semiconductors) and silicon integrated circuits. Indeed, recent development in optoelectronic integrated circuits (OEICs) enables us to implement light-emitting devices (LEDs) on silicon substrate by controlling defects at III–V/silicon interface. For example, Furukawa et al. demonstrated that lattice-matched and defect-free GaPN epilayers can be grown on silicon with a thin GaP buffer layer [20]. The task is enormous and as a practical matter only small scale OEICs have been demonstrated. While the integration levels of III–V OEICs have remained low, the degree of integration in commercial GaAs integrated circuits has reached VLSI levels in recent years. These advances offer a route to achieving much higher levels of optoelectronic integration through epitaxial growth of III–V heterostructures on GaAs-based VLSI electronics.

Most experimental prototypes of chemical excitable computing devices suffer from difficulties with representation of results of wave interaction. This is because being excited a medium's micro-volume becomes refractory and then recovers back to the resting state. Excitation wave-fronts usually annihilate in the result of collision. Therefore, experimental excitable RD computers require some external devices, like digital camera, to record their spatio-temporal dynamics. Thus, e.g. to compute a collision-free path around obstacles in thin-layer BZ-medium one must record snapshots of BZ-medium's activity and then analyze this series of snapshots to extract results of the computation [8,10]. This is the cost we pay for reusable (because the excitable medium eventually returns to resting state) RD processors. Another option of preserving results of computation may be to employ non-excitable RD media, where a precipitate is formed (or do not formed) in the result of diffusion wave interaction with a substrate (or competition of several wave fronts for the substrate) [4,5,7,17]. Precipitation is an analog of infinite memory. The feature is priceless however makes experimental prototypes simply disposable, in contrast to excitable media the precipitate-forming media can be used just once.

RD semiconductor computers, because they are essentially man-made devices, may allow us to combine reusability and rich space–time dynamics of excitable RD media with low post-processing costs of precipitate-forming RD media. This can be done by embedding a lattice of oscillatory p–n–p–n elements into a lattice of excitatory p–n–p–n elements. The excitatory elements (EEs) will form a substrate to support traveling excitation waves while oscillatory elements (OEs) will play a role of rewritable memory. For example, to represent sites of wave-front collision we must adjust an activation threshold of OEs in such manner that front of a single wave will not trigger OEs, however when two or more wave-fronts collide the OEs at the sites of collision are triggered and continue oscillate even when the wave-fronts annihilate.

What computational tasks can be realized in RD semiconductor devices? Most primitive operations of image processing (see overview in [2]), e.g. detection of contour and enhancement, are straightly mapped onto the silicon architecture. Silicon implementation of RD (precipitate formation based) algorithms for computational geometry—Voronoi diagram [5,17,18] and skeletonization [3]—requires embedding of oscillatory elements in the lattice of excitatory p–n–p–n devices; the oscillating elements will represent bisectors of a Voronoi diagram and segments of a skeleton.

Universal computation can be realized in RD semiconductor devices using two approaches. Firstly, by employing collision-based mode of computation in excitable media [9], where functionally complete sets of Boolean gates are implemented by colliding waves. In collision-based mode, however we must force the medium to be in a sub-excitable regime which may pose some problems from fabrication point of view. Secondly, we can 'physically' embed logical circuits, namely their diagram-based representations, into the excitable medium [39,43]. In this we employ particulars of photo-response of p–n–p–n elements and project the logical circuit onto the medium as pattern of heterogeneous illumination.

5. Conclusion

We proposed a massive parallel computing device [11,12] based on principles of information processing in reaction–diffusion (RD) chemical media [1,2]. This novel silicon device imitates auto-catalytic and dissipative phenomena of the chemical RD systems, however comparing to real chemical medium the semiconductor analog of RD computers, functions much faster. We studied operational characteristics of the RD silicon devices and demonstrate feasibility of the approach on several computational tasks. Our results indicate that the proposed RD device will be a useful tool for developing novel hardware architectures based on RD principles of information processing.

Acknowledgements

This study was supported by the "Analog Reaction–Diffusion Chip: The Development of Functional LSIs recovering Fingerprint Images" in '00 from the New Energy and Industrial Technology Development Organization (NEDO) of Japan.

References

[1] Adamatzky A. Reaction–diffusion and excitable processors: a sense of the unconventional. In: Parallel and distributed computing: theory and practice (Special Issue: Unconventional Parallel Architectures), vol. 3. 2000. p. 113–32.
[2] Adamatzky A. Computing in nonlinear media and automata collectives. Bristol: Institute of Physics Publishing; 2001.
[3] Adamatzky A, De Lacy Costello B, Ratcliffe NM. Experimental reaction–diffusion pre-processor for shape recognition. Phys Lett A 2002;344–352:297.
[4] Adamatzky A, De Lacy Costello BPJ. On some limitations of reaction–diffusion computers in relation to Voronoi diagram and its inversion. Phys Lett A 2003;309:397–406.
[5] Adamatzky A, Tolmachiev D. Chemical processor for computation of skeleton of planar shape. Adv Mater Opt Electron 1997;7:135–9.
[6] Adamatzky A, De Lacy Costello B, Melhuish C, Ratcliffe N. Experimental reaction–diffusion chemical processors for robot path planning. J Intell Robotic Syst 2003;37:233–49.
[7] Adamatzky A, De Lacy Costello BPJ. Experimental logical gates in a reaction–diffusion medium: The XOR gate and beyond. Phys Rev E 2002;66:046112.
[8] Adamatzky A, De Lacy Costello BPJ. Collision-free path planning in the Belousov–Zhabotinsky medium assisted by a cellular automaton. Die Naturwissenschaften 2002;89:474–8.
[9] Adamatzky A. Universal dynamical computation in multi-dimensional excitable lattices. Int J Theor Phys 1998;37:3069–108.
[10] Agladze K, Magome N, Aliev R, Yamaguchi T, Yoshikawa K. Finding the optimal path with the aid of chemical wave. Physica D 1997;106:247–54.
[11] Asai T. Reaction–diffusion systems on silicon. Trans Inst Electrical Eng Jpn 2001;121:253–7.
[12] Asai T, Nishimiya Y, Amemiya Y. A CMOS reaction–diffusion circuit based on cellular-automaton processing emulating the Belousov–Zhabotinsky reaction. IEICE Trans Fundament Electron, Commun Comput 2002;E85-A:2093–6.
[13] Beato V, Engel H. Pulse propagation in a model for the photosensitive Belousov–Zhabotinsky reaction with external noise. In: Schimansky-Geier L, et al., editors. Noise in complex systems and stochastic dynamics: Proceedings of SPIE, vol. 5114. 2003. p. 353–62.
[14] Blittersdorf R, Müller J, Schneider FM. Chemical visualization of boolean functions: a simple chemical computer. J Chem Educ 1995;72:760–3.
[15] Brandtstädter H, Braune M, Schebesch I, Engel H. Experimental study of the dynamics of spiral pairs in light-sensitive Belousov–Zhabotinskii media using an open-gel reactor. Chem Phys Lett 2000;323:145–54.
[16] Conrad M, Zauner KP. Molecular computing with artificial neurons. Commun Korea Inform Sci Soc 2000;18:78–89.
[17] De Lacy Costello B, Adamatzky A. On multitasking in parallel chemical processors: experimental findings. Int J Birfur Chaos 2003;13:521–33.
[18] De Lacy Costello B, Adamatzky A, Ratcliffe N, Zanin AL, Liehr AW, Purwins HG. The formation of Voronoi diagrams in chemical and physical systems: experimental findings and theoretical models. Int J Bifur Chaos, in press.
[19] Flessels JM, Belmonte A, Gáspár V. Dispersion relation for waves in the Belousov–Zhabotinsky reaction. J Chem Soc Faraday Trans 1998;94:851–5.
[20] Furukawa Y, Yonezu H, Ojima K, Samonji K, Fujimoto Y, Momose K, et al. Control of N content of GaPN growun by molecular beam epitaxy and growth of GaPN lattice-matched to Si (1 0 0) substrate. Jpn J Appl Phys 2001;41:528–32.
[21] Grill S, Zykov VS, Müller SC. Spiral wave dynamics under pulsatory modulation of excitability. J Phys Chem 1996;100:19082–8.
[22] Hjelmfelt A, Weinberger ED, Ross J. Chemical implementation of neural networks and Turing machines. Proc Natl Acad Sci USA 1991;88:10983–7.
[23] Hjelmfelt A, Weinberger ED, Ross J. Chemical implementation of finite-state machines. Proc Natl Acad Sci USA 1992;89:383–7.
[24] Hjelmfelt A, Ross J. Mass-coupled chemical systems with computational properties. J Phys Chem 1993;97:7988–92.
[25] Hjelmfelt A, Schneider FW, Ross J. Pattern recognition in coupled chemical kinetic systems. Science 1993;260:335–7.
[26] Hjelmfelt A, Ross J. Implementation of logic functions and computations by chemical kinetics. Physica D 1995;84:180–93.
[27] Kuhnert L, Agladze KL, Krinsky VI. Image processing using light-sensitive chemical waves. Nature 1989;337:244–7.
[28] Mohajerzadeh S, Nathan A, Selvakumar CR. Numerical simulation of a p–n–p–n color sensor for simultaneous color detection. Sensor Actuator A 1994;44:119–24.
[29] Motoike NI, Yoshikawa K. Information operations with multiple pulses on an excitable field. Chaos, Solitons & Fractals 2003;17:455–61.
[30] Motoike NI, Yoshikawa K, Ighuchi Y, Nakata S. Real-time memory on an excitable field. Phys Rev E 2001;63:036220.
[31] Motoike I, Yoshikawa K. Information operations with an excitable field. Phys Rev E 1999;59:5354–60.

[32] Nicolis G, Prigogine I. Self-organization in nonequilibrium systems—from dissipative structures to order through fluctuations. New York: John Wiley & Sons, Inc.; 1977.
[33] Niedernostheide FJ, Kreimer M, Schulze HJ, Purwins HG. Periodic and irregular spatio-temporal behaviour of current density filaments in Si p^+–n^+–p–n^- diodes. Phys Lett A 1993;180:113–8.
[34] Niedernostheide FJ, Kreimer M, Kukuk B, Schulze HJ, Purwins HG. Travelling current density filaments in multilayered silicon devices. Phys Lett A 1994;191:285–90.
[35] Petrov V, Ouyang Q, Swinney HL. Resonant formation in a chemical system. Nature 1997;388:655–7.
[36] Rambidi NG. Neural network devices based on reaction–duffusion media: an approach to artificial retina. Supramol Sci 1998;5:765–7.
[37] Rambidi NG, Yakovenchuk D. Chemical reaction–diffusion implementation of finding the shortest paths in a labyrinth. Phys Rev 2001;E63:0266071–6.
[38] Rambidi NG, Shamayaev KE, Peshkov GY. Image processing using light-sensitive chemical waves. Phys Lett A 2002;298:375–82.
[39] Steinbock O, Toth A, Showalter K. Navigating complex labyrinths: optimal paths from chemical waves. Science 1995;267:868–71.
[40] Sze SM. Physics of semiconductor devices. New York: Wiley & Sons; 1981.
[41] Schebesch I, Engel H. Wave propagation in heterogeneous excitable media. Phys Rev E 1998;57:3905–10.
[42] Tóth Á, Gáspár V, Showalter K. Propagation of chemical waves through capillary tubes. J Phys Chem 1994;98:522–31.
[43] Tóth A, Showalter K. Logic gates in excitable media. J Chem Phys 1995;103:2058–66.
[44] Vittoz EA. Micropower techniques. In: Tsividis Y et al., editors. Design of MOS VLSI circuits for telecommunications. New Jersey: Prentice-Hall; 1985. p. 104–44.
[45] Wang J. Light-induced pattern formation in the excitable Belousov–Zhabotinsky medium. Chem Phys Lett 2001;339:357–61.
[46] Yoneyama M. Optical modification of wave dynamics in a surface layer of the Mn-catalyzed Belousov–Zhabotinsky reaction. Chem Phys Lett 1996;254:191–6.
[47] Zauner KP, Conrad M. Molecular approach to informal computing. Soft Comput 2001;5:39–44.